Neural Computing and Applications (2022) 34:1541–1555
https://doi.org/10.1007/s00521-021-06497-3

ORIGINAL ARTICLE

Failure assessment of defected pipe under strike-slip fault with data-driven models accounting for the model uncertainty

Hieu Chi Phan[1] · Nang Duc Bui[1]

Received: 24 January 2021 / Accepted: 30 August 2021 / Published online: 10 September 2021

Abstract
Buried pipeline is threatened from the soil displacement due to earthquake and other causes, which leads to the formation of unexpected external forces such as bending moment. The problem can be worse with the appearance of defects, resulting in the reduction in pipe capacity. The paper focuses on the overall problem of defected pipe crossing the strike-slip fault. A full-scaled FE model can be very complicated with the large-scale and micro-scale levels corresponding to the strike-slip fault and defect on pipe problems, respectively. To ease this difficulty, the macro and micro problems are solved separately with two types of FE models and their corresponding databases. To be specific, one FE model is used for predicting external moment due to strike-slip fault and the other is for predicting the moment capacity of defected pipe. Data-driven models are consequently developed with artificial neural network (ANN) for each database generated from these types of models: *ANN1* evaluating moment capacity of defected pipe (R^2 is 0.9943 on test set) and *ANN2* predicting both moment and axial force appeared in pipe due to strike-slip fault (R-squares are 0.9883 and 0.9929 on test set, respectively). Consequently, the stress–strength analysis for the overall problem is solved. Accounting for the unavoidable uncertainty of the models, the paper proposed an approach which assumes that the actual distribution of residual of a model is equivalent to this of the test set. The distributions of residuals on test set of these ANNs are tested to be normally distributed and generated by the conventional Monte Carlo simulation. To the end, the deterministic problem leads to the failure probability. The proposed framework has been investigated, and the final results on this selective parametric study are reasonable.

Keywords Defected pipe · Bending capacity · Data-driven model · Finite element analysis · Strike-slip fault · Model uncertainty

1 Introduction

Earthquake causes strike-slip (or normal) fault in soil, and to its turn, this phenomenon leads to the bending moment and axial force in buried pipeline. A conventional stress–strength problem then merges with the desire of capturing the behavior of the pipeline under such conditions. Various studies have been developed including the analytical and numerical methods to assess the stress, strain or internal forces appeared in the pipes. The conventional approach is modeling the problem with the 2D beam placed in elastic spring soil [1–4]. The evolution in developing models for this problem is mainly to deal with geometric [3] or material nonlinearities [2, 4, 5]. Additionally, the nonlinear properties of soil are sometimes taking into account as in [6].

While the analytical method has a critical drawback of hardly adapting to the increase in complexity of these models, the finite element analysis (FEA) is able to solve these difficulties and provides the insights into the nonlinear behavior of the model ([7–9]) such as local buckling phenomenon [10, 11]. However, both analytical and FE methods have the unify concern of simplifying their models for practical applications. For instance, Karamitros et al. [2] improve their previous study [1] for the sake of simplicity; Trifonov and Cherniy proposed model which applied adjustments on the previous models with additional

✉ Nang Duc Bui
ducnangbui@lqdtu.edu.vn

[1] Le Quy Don Technical University, 236 Hoang Quoc Viet, Hanoi 100000, Vietnam

strong assumptions [12]; and the formation of plastic hinge is used in the FE analysis with commercial software for the same purpose [13]. These studies are developed for intact pipe only, which preserves the perfect geometric dimension as newly manufactured. Unfortunately, the practical problem of pipeline fault crossing can be much more complicated with the appearance of defects due to working in corrosive environment.

The appearances of advert effect of corrosion are focused in many studies. For instance, Folkman [14] reported that the corrosion is secondly ranked as the most common cause of pipe break. Similar to the buckling in which the local defects are not affected much to the overall structures, localized defects can be ignored from the macro perspective where the internal forces (i.e., bending moment and axial force) are formed based on the pipe and soil interaction and their stiffness rather than governed by the appearance of localized defects. However, pipe capacity, specially the burst pressure for defected pipe [15–18], can be seriously reduced with the occurrence of corrosion. And thus, analyzing an intact pipe is insubstantial for this scenario.

In practice, crossing a fault causes the appearance of the bending moment and axial force in pipe with capacity reduced by the localized reduction in wall thickness [19–23]. Mondal and Dhar [19] use the Abaqus software to establish the loci of bending defected pipe with the appearance of axial load and internal pressure. Liu et al. [20] provide a thorough investigation of behavior of defected pipe under the bending moment with the incorporation of experiment and simulation. Safety assessment of such structure is investigated regarding multiple defects and their various shapes in [21]. Phan et al. [23] develop a data-driven model based on FE database for such structures. This approach recently becomes popular ([24, 25]) because of (1) the convenience due to the reduction of cumbersome work required for FEAs and (2) the avoidance of rigid assumption made by analytical model. Furthermore, when experiment results are substantial, data-driven models can provide quality predictions [26–28]. However, a problem can be raised with the data-driven approach: the difficulty in quantifying model uncertainty.

Apparently, quantifying model uncertainty is practically desired for engineering applications [29]. In general, statistical tools and probability method are powerful in assessing the uncertainty of the models. Various attempts have been made to observe the performance of model including the uncertainty. Amaya-Gómez et al. [18] have validated 22 models with the ratio of predict/experiment of about 70–80 percent and coefficient of variances of up to 0.31. Keshtegar et al. [17] have revealed a significant high mean absolute error of more than 30 models compared to experiment and simulation results. Using the validation metrics such as coefficient of determination, R^2, mean absolute error, MAE, or mean square error on the train and test set is the conventional approach to evaluate the performance of the developed model. Given that the actual value of the prediction is unknown, these metrics provide an approximation for model error and uncertainty [23–28]. To limit the phenomenon of quality—decrease of the data-driven models, Phan et al. [30] have illustrated the effect of the out-of-boundary prediction which is analogous to extrapolations if the inputs are out of their max–min ranges established by the database. Along with the observation on evaluation metrics, this is a practical approach to limit the uncertainty and error of the model [23–25, 31]. However, none of the aforementioned studies regards to the combination of multiple models and the uncertainty of this incorporation.

In this paper, the stress–strength analysis of the defected pipe under the strike-slip fault is focused based on two constituent ANN models: The first one, *ANN1*, predicts the moment capacity of defected pipe and the other, *ANN2*, estimates the internal forces appeared due to the fault including the bending moment and corresponding axial force. To quantify the model uncertainty, the paper proposed a framework using the residual values on test set as the alternative for the actual residuals. Once this assumption is applied, the final predicted variables are failure probability, P_f, of the structural system. The conventional Monte Carlo simulation (MCS) is chosen due to the simplicity and reliability of this method in assessing the failure probability. Finally, various case studies are investigated as the selective parametric study.

2 Materials and methods

2.1 Modeling the interested structures with FE

2.1.1 The moment capacity of defected pipe with axial load

As aforementioned, two models are established in this study. In the first model, the moment capacity of a defected pipe, M_{cap}, coupled with the combination of the axial force, N, is considered. The inputs of this model can be categorized as: pipe dimensions, defect dimensions and material properties. The pipe dimensions are pipe diameter, D, and wall thickness, t, which are normalized to the ratio of t/D. With the randomness of defect dimensions (Fig. 1a), the common assumption is to idealize it to be a squared and sharp-edge defect as in Fig. 1b ([15, 19, 21, 32]). This assumption leads to the defect dimensions which are depth of defect, d, length of defect, l, and width of the defects, w_{arc}. Additionally, ratio of moment in x- and y-axis, M_y/M_x,

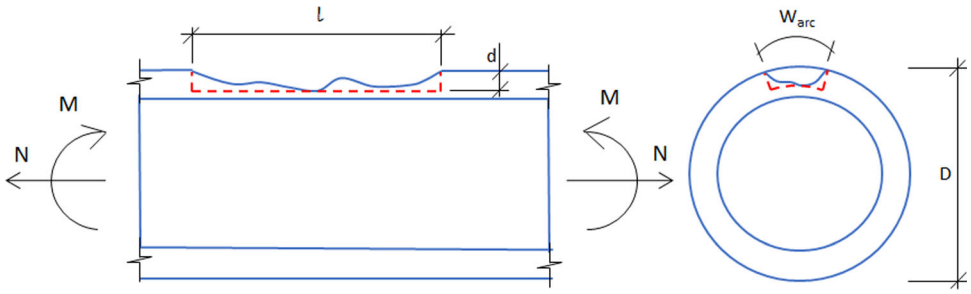

Fig. 1 The simplified model for corroded pipe problem

is added accounting for the out-of-bending-plane scenarios. The input designated as α presented the direction of moment along the x-axis; if M_x is positive, then α is 0, and α is π if M_x is negative.

The bilinear model for pipe material is chosen in this study with the elastic state preceded by the hardening state ([20, 33–36], Fig. 2). The inputs within the material groups are the yield stress/strain (σ_y/ε_y) and the ultimate stress/strain (σ_u/ε_u). Summary of these inputs is given in Table 1.

Consequently, the defected pipe is then modeled in Abaqus[R] as provided in Fig. 3. The study inherits the results from our preliminary study [23] with the quarter model (Fig. 3a) suggested in [19]. This model includes a system of symmetric constrains at across and along the pipe. At the cut across the defect, the symmetric constrain has $U_3 = UR_1 = UR_2 = 0$, where U_3, UR_1, UR_2 are the longitudinal displacement and rotations to the x- and y-axis, respectively. Other two constrains are applied along the cuts through the pipe center with $U_1 = UR_2 = UR_3 = 0$. The applied moment is placed at the other end of the pipe with the multiple points constrain (MPC).

Due to the symmetric property, the quarter model is only applicable for the cases where the defect is located in the bending plane (i.e., the most severe situation). To increase the range of the data-driven models, the half model has been implemented with only symmetric constrain across the cut section (Fig. 3b). The C3D8R element type is used for these models with elements surrounding the defect that are densely divided.

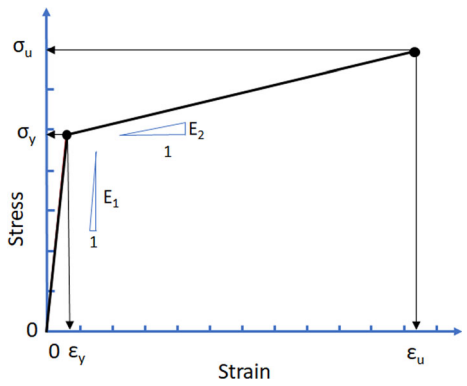

Fig. 2 Bilinear material model for steel

These models are validated with results of analytical methods proposed by Zheng et al. [37] and Chen et al. [38], and the results are given in Fig. 4. It is worth to remind that models of Zheng et al. and Chen et al. use plastic-perfect material. With the use of the ultimate tensile strength as the flow stress, these models are over-estimated compared to the bilinear model chosen in this study. Additionally, the appearance of the samples with defects located out of the bending plane leads to the under-estimation of the analytical models. This is observed in Fig. 4b where only pipe with defect in the bending plane is shown, and most of data points are above the 1:1 line, which indicates the effect of difference in the material models to the prediction of pipe capacity. This provides a validation of the present FE model to analytical models where the differences may exist but the overall predictions are acceptable.

2.1.2 Pipe crossing the transverse fault

In the second model, the interested variables are the forces appeared due to the applied strike-slip fault in a buried pipe (Fig. 5). To be specific, these forces are the peak moment, M_{peak}, and the corresponding axial force, N_{cor}. Analogous to the overall buckling phenomenon where the appearance of the defects or holes can be ignored, the defect on pipe in this case is assumed to have minor effect to M_{peak} and N_{cor}. Consequently, the amount of displacement, the relative stiffness and the interaction of the pipe and soil are the main factors for the formation of M_{peak} and N_{cor}.

To simulate the fault, the soil in a half space horizontally displaces parallel to the fault trace. Meanwhile, the remaining soil space is stable. Under this displacement, the soil can be considered as the continuous springs along the pipe with Winkler foundation model. The springs belonging to the moving part are moving with a quantity of f. Such fault displacement, f, which establishes a β angle to the pipe, can be decomposed to f_x and f_y corresponding to x- and y-axis. This type of model is widely used in both analytical (e.g., [1–3, 12, 39]) and numerical (e.g., [4, 13, 40–42]) methods due to its simplicity.

Table 1 Collected properties of metal materials

Material	σ_y (MPa)	σ_u (MPa)	ε_y –	ε_u –	E_1 (MPa)	E_2 (MPa)	Reference
Steel, X42	290	415	0.0014	0.1036	207,143	1223	[20]
Steel, X52	375	468	0.0018	0.2230	208,333	420	[33]
Steel, X60_1	452	542	0.0021	0.043	215,238	2200	[34]
Steel, X60_2	414	600	0.0020	0.095	207,000	2000	[34]
Steel, X65	464.5	563.8	0.0022	0.061	211,136	1689	[35]
Steel, X70_1	508	667	0.0024	0.095	211,667	1717	[36]
Steel, X70_2	523	701	0.0025	0.095	209,200	1924	[36]
Steel, X80	524	685	0.0025	0.078	209,600	2132	[36]

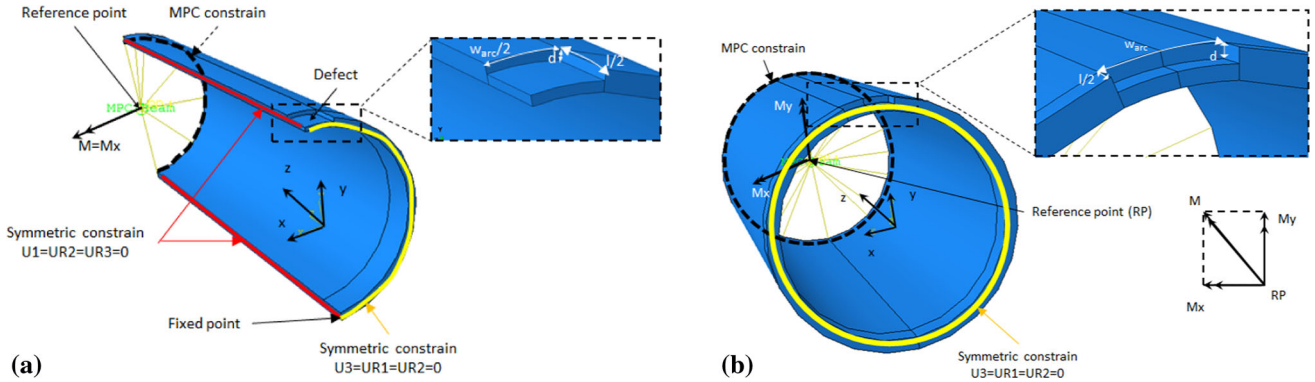

Fig. 3 The finite element model for ANN1 predicting defected pipe capacity

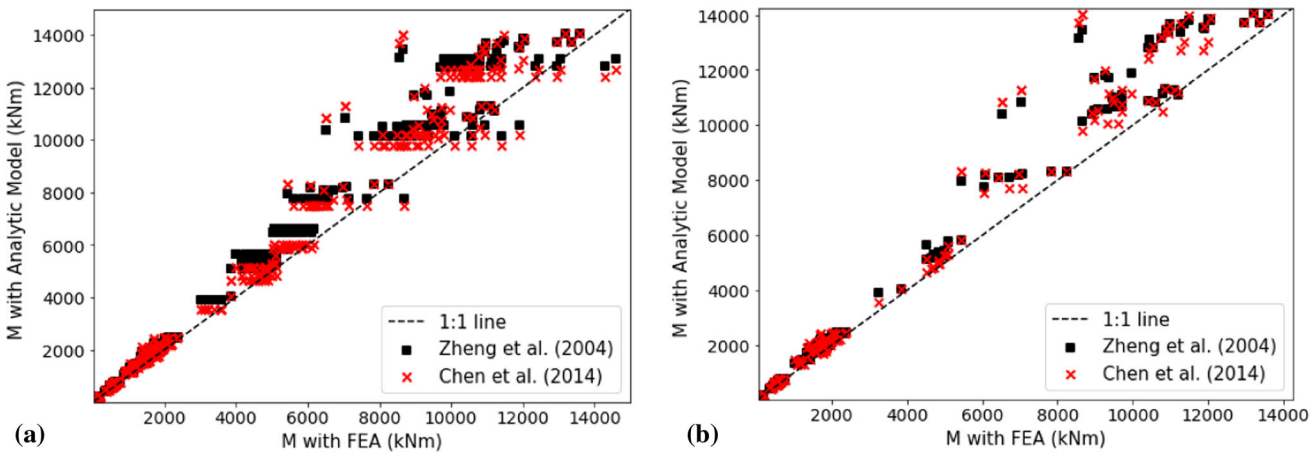

Fig. 4 Comparison of FE model versus analytical models in [37, 38] for **a** all databases and **b** the cases that defects are in the bending plane only

The Abaqus[R] as in Fig. 6 used in this study with the pipe–soil interaction (PSI) element is widely used to capture the soil effect on pipe. Two rigid surfaces are attached to one end of the PSI elements, and one of them will be displaced with a quantity f and angle β to the horizontal axis. A 1000-m-length pipe is attached to the other side of the PSI elements by 2D pipe-type elements, PIPE21. The middle 100 m length of the pipe is densely divided into 200 and 2000 elements for pipe with diameter larger and less than 200 mm, respectively. The rest of the pipe is also divided into 200 elements if D is larger than 200 mm and 2000 elements if D is less than 200 mm.

The springs represented for soil are commonly considered to be linearly elastic as issued in ASCE standard [43]. In this study, soil properties are simplified with four variables, including: transverse horizontal direction yield force, P_T; transverse horizontal direction yield displacement, y_T; axial direction yield force, P_a; and axial direction yield displacement, y_a (Fig. 7).

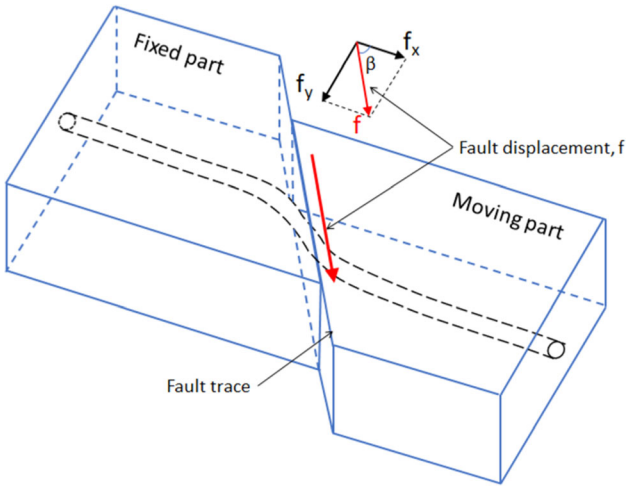

Fig. 5 Pipeline crossing transverse fault

The FE model is validated with results from Talebi et al. [3] to observe the difference in calculating peak moment and peak axial force. It can be seen that the two models are well matched and the critical trend of the increase in peak forces within the change in the fault displacement can be observed (Fig. 8).

2.2 Developing data-driven models

The conventional ANN, which is widely used in the literature for the regression problems as in [25, 44, 45], is chosen in this study for developing data-driven models. For the sake of simplicity, the fundamental of this machine learning model is not discussed in detail. Instead, discussion on the input system, boundaries, post-training processes, observation on the described statistics and the statistical tests on residual is focused. The first ANN model, *ANN1*, aims to predict moment capacity of defected pipe (i.e., M_{cap}), and the second model, *ANN2*, targets to estimate the internal forces (both M_{peak} and N_{cor}) in pipe due to transverse fault.

Obviously, the inputs of the stress–strength problem are the union of these from constituent models. The input will be categorized as: pipe dimensions, defect dimensions, soil properties and strike-slip fault properties groups. Pipe dimension inputs (D and t) and material inputs (σ_y, ε_y, σ_u and ε_u) are the two groups that will be shared between the ANN models. Defect dimension group (d, l, w_{arc}, α and M_y/M_x) will be used in *ANN1* only. The inputs in the soil properties group (P_a, y_a, P_t, y_t) and strike-slip fault group (f_x and f_y) will be needed for prediction with *ANN2*.

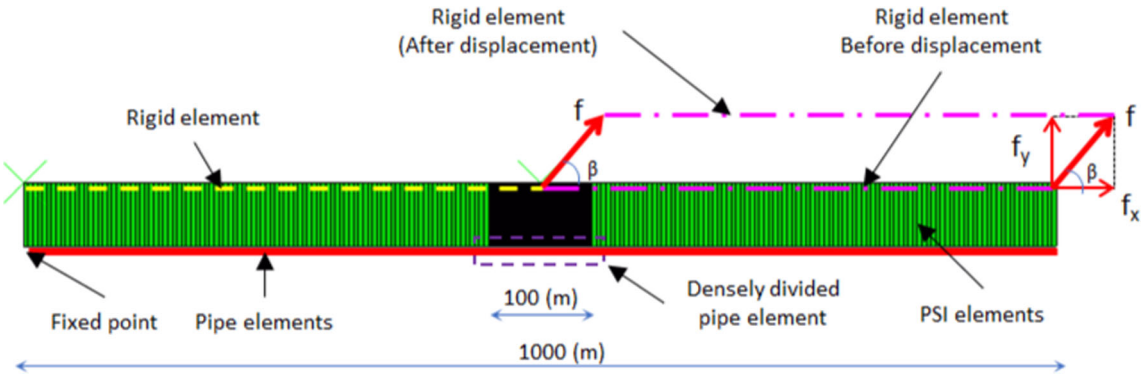

Fig. 6 The finite element model for ANN2 predicting the internal forces in pipe

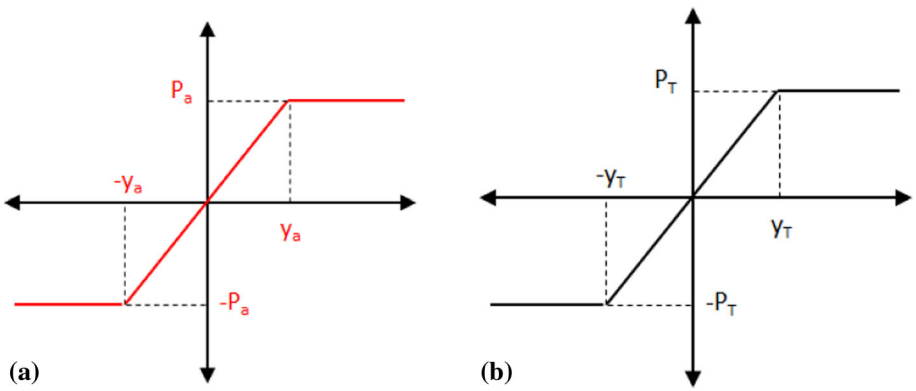

Fig. 7 Force–displacement perfectly plastic properties of soil springs

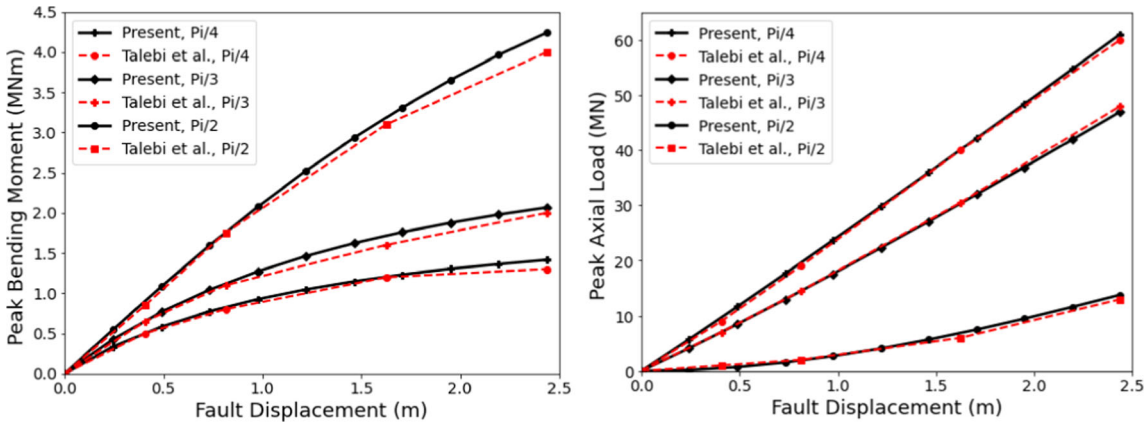

Fig. 8 Validation on the fault displacement versus peak bending moment and axial force of the present study with Talebi et al. [3]

Illustration of inputs used for each data-driven model is given in the "input block" in Fig. 10. It is worthy noted that the *ANN1* requires the axial load, N, which will be extracted from the corresponding axial load, N_{cor}—an output of the *ANN2*. The interaction between these two data-driven models is consequently required where the output of a model is used as the input of the other. For the overall valid prediction, boundaries of each input must be the intersection of those from *Databases 1 and 2*. This interaction will be discussed further in Sect. 2.3.

The model training process is implemented conventionally with the databases which are divided into train and test sets with the ratios of 0.8 and 0.2, respectively. The error (*MSE* in this paper) of model on the train set is used as the loss function, and the evaluation metrics on the test set are used for observing the performance of the models on unfamiliar inputs. Additionally, the distributions of the residuals on test sets of *ANN1* and *ANN2* are investigated and statistically tested to confirm the validation of consequent MCS implementation with known distributions.

2.3 Combinations of data-driven models for the stress–strength analysis with model uncertainties

As above discussion, a problem will arise with the combination of models for pipe capacity and internal forces in pipes because each model has error or uncertainty itself. Once a set of inputs is fed for the ANN, the predicted output is a deterministic value. However, the error of such prediction statistically occurs and the quantity is depending on the accuracy of the data-driven model. Assuming that the residuals of models are obtained and followed any type of distribution, the interested variables can be considered as the random variables: $\widetilde{M}_{\text{cap}}$, $\widetilde{M}_{\text{peak}}$ and $\widetilde{N}_{\text{cor}}$ in Eqs. 1, 2 and 3, respectively. These random variables have the corresponding means and standard deviations: $M_{\text{cap,mean}}$, $M_{\text{cap,std}}$; $M_{\text{peak,mean}}$, $M_{\text{peak,std}}$; $N_{\text{cor,mean}}$, $N_{\text{cor,std}}$.

$$\widetilde{M}_{\text{cap}} = \text{rand}\left(M_{\text{cap,mean}}, M_{\text{cap,std}}\right) = M_{\text{cap,pred}} + \widetilde{r}_{\text{cap}} = M_{\text{cap,pred}} + \text{rand}\left(r_{\text{cap,mean}}, r_{\text{cap,std}}\right) \quad (1)$$

$$\widetilde{M}_{\text{peak}} = \text{rand}\left(M_{\text{peak,mean}}, M_{\text{peak,std}}\right) = M_{\text{peak,pred}} + \widetilde{r}_{\text{peak}} = M_{\text{peak,pred}} + \text{rand}\left(r_{\text{peak,mean}}, r_{\text{peak,std}}\right) \quad (2)$$

$$\widetilde{N}_{\text{cor}} = \text{rand}\left(N_{\text{cor,mean}}, N_{\text{cor,std}}\right) = N_{\text{cor,pred}} + \widetilde{r}_{\text{cor}} = N_{\text{cor,pred}} + \text{rand}\left(r_{\text{cor,mean}}, r_{\text{cor,std}}\right) \quad (3)$$

where $M_{\text{cap,pred}}$, $M_{\text{peak,pred}}$ and $N_{\text{cor,pred}}$ are the moment capacity of the defected pipe predicted with *ANN1*, moment capacity and corresponding axial load of the defected pipe predicted with the *ANN2*, respectively; $\widetilde{r}_{\text{cap}}$, $\widetilde{r}_{\text{peak}}$ and $\widetilde{r}_{\text{cor}}$ are random residuals of moment capacity of defected pipe, peak moment and axial load in pipe, respectively; $r_{\text{cap,mean}}$ and $r_{\text{cap,std}}$ are the actual mean and standard deviation of residual of *ANN1* predicting M_{cap}, respectively; $r_{\text{peak,mean}}$ and $r_{\text{peak,std}}$ are the actual mean and standard deviation of residual of *ANN2* predicting M_{peak}, respectively; and $r_{\text{cor,mean}}$ and $r_{\text{cor,std}}$ are the actual mean and standard deviation of residual of *ANN2* predicting N_{cor}, respectively.

Given that the actual distributions of residuals are unknown, an assumption is made in this paper that: "The distribution of the actual residual and the distribution of residual on the test set are equivalent." With this assumption, the distributions of the actual residuals can be replaced by the residuals found from the test set. Once this assumption is set, the conventional stress–strain problem can be solved by conventional reliability methods such as FORM or Monte Carlo simulation (MCS) (e.g., [46–48]). In this paper, the conventional MCS is implemented where the distributions of the inputs are known for generating a substantial number of trials to figure out the failure probability (Fig. 9).

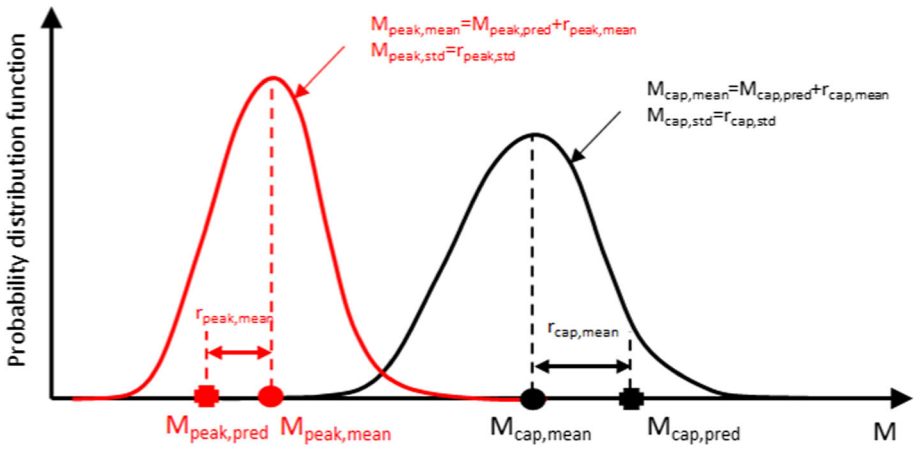

Fig. 9 Predicted values of ANN models and corresponding uncertainties

The framework of the paper is given in Fig. 10. The molecular blocks are the *"input block,"* the *"internal force block"* and the *"capacity block."* The *"input block"* simply deals with synchronizing and providing usable inputs for developed models in the *"internal force block"* and *"capacity block."* Because inputs for each data-driven models should be within their boundaries ([23–25]), checking operations are placed before feeding inputs to *ANN1* and *ANN2* models. Consequently, the residual distributions on the test set of these models are found and statistically tested to find their distributions for further MCS implementations. The procedure will be terminated if the type of distribution for the residuals cannot be found (i.e., fail the statistics tests). If the tests are satisfied, the first MCS, *MCS1*, is conducted with n values of samples to obtain $\widetilde{M}_{\text{peak}}$ and $\widetilde{N}_{\text{cor}}$ from M_{peak}, N_{cor} and their corresponding residuals. $\widetilde{N}_{\text{cor}}$ is then normalized by N_o in Eq. 4 and sent to *ANN1* as input to generate $n \times M_{\text{cap}}$ by the second MCS, *MCS2*. Consequently, n values of M_{cap} and M_{peak} are compared and the probability of failure, P_f, is finally found with the failure counting process. Given that *ANN1* and *ANN2* are obtained, the pseudo-code for the process is also provided in the following.

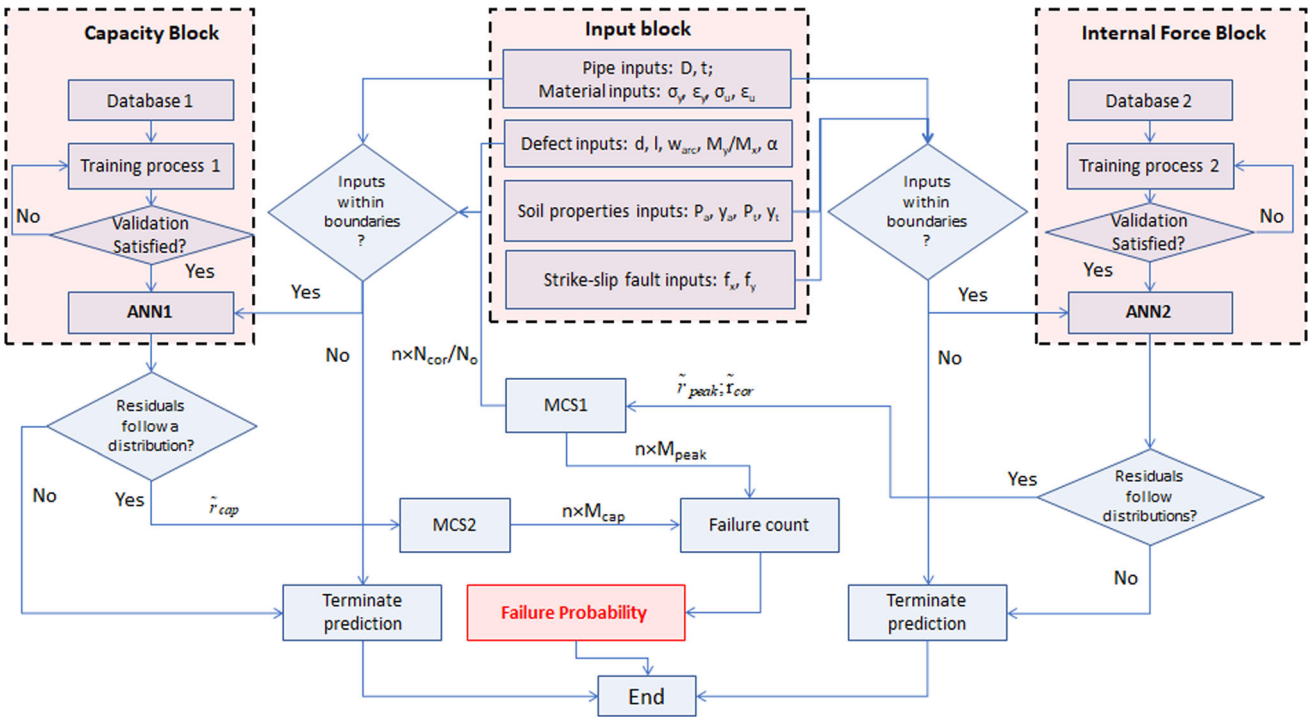

Fig. 10 Flowchart of incorporating ANN models accounting for the model uncertainties

Input: Deterministic: D, t/D, d/t, l/D, w_{arc}/D, σ_y, σ_u, ε_y, ε_u, α, M_y/M_x, f_y/D, f_x/D, P_a, y_a, P_t, $\tilde{r}_{cap}$, $\tilde{r}_{peak}$, $\tilde{r}_{cor}$.

Output: P_f

Begin

Step 1: $n \leftarrow 10^6$

Step 2: *Input A* $\leftarrow 1\times[D, t/D, \sigma_y, \sigma_u, \varepsilon_y, \varepsilon_u, f_y/D, f_x/D, P_a, y_a, P_t, y_t]$;

Step 3: $1\times[M_{peak,pred}, N_{cor,pred}] \leftarrow$ *ANN2* and *Input A*;

Step 4: *MCS1*: $n\times[M_{peak}, N_{cor}] \leftarrow$ Eq.2, 3 and $\tilde{r}_{cap}$;

Step 5: $N_o \leftarrow$ Eq.4 and D, t, σ_u;

Step 6: *Input B* $\leftarrow n\times$[Deterministic: D, t/D, d/t, l/D, w_{arc}/D, σ_y, σ_u, ε_y, ε_u, α, M_y/M_x; Random: $N_{cor,pred}/N_o$];

Step 7: $n \times M_{cap,pred} \leftarrow$ *ANN1* and *Input B*;

Step 8: *MCS2*: $n \times M_{cap} \leftarrow$ Eq.1, $n \times M_{cap,pred}$, $\tilde{r}_{peak}$ and $\tilde{r}_{cor}$;

Step 9: f=0;

Step 10: For i in [1:n]:

If the ith M_{cap} < the ith M_{peak}:

$f = f + 1$;

End

Step 11: $P_f = f/n$

End

3 Results

3.1 Performance of proposed data-driven models

As aforementioned, two databases, designated as *Database 1* and *Database 2*, have been developed in this study. *Database 1*, developed for *ANN1* model predicting M_{cap}, contains up to 778 samples. Meanwhile, *Database 2* with 358 samples is for *ANN2* to predict M_{peak} and N_{cor}. Some features are normalized to increase the range of models. To be specific, t, l and w_{arc} are normalized with D and d, N and M_y are divided into t, N_o, M_x, respectively.

A wide range of pipes from 100 to 1219 mm are included in *Database 1* with the ratio of wall thickness to outer diameter from 0.0113 to 0.100. Meanwhile, *Database 2* contains only intact pipes from 100 to 1200 mm with the earlier discussion/assumption that: the localized defects on pipe have no effect on the formation of moment in the strike-slip fault problem. With this assumption, the defect dimension inputs (d, l,w_{arc}) and location inputs (α *and* M_y/M_x) only appeared in *Database 1*. The maximum depth of defect in this database is up to 80% of the wall thickness (i.e., holes are not formed).

Pipe materials in this study are steel with various grades ranging from X42 to X80 (Table 1). Properties of soil spring are only in *Database 2* with the ranges referred from [42]. The normalized axial force (i.e., N/N_o in *Database 1* and N_{cor}/N_o in *Database 2*) in D*atabase 2* is much narrower than in *Database 1* (with [− 0.1371, 0.2752] compared to [− 0.8070, 0.9120], respectively). Consequently, ranges of N/N_o are used as the boundaries for the overall problem. To the end, moment capacity of defected pipe, M_{cap}, in *Database 1* ranges from 0 (or failure due to the axial load) to 13.58 MNm compared to M_{peak} in *Database 2* which ranges within [3.64×10^{-4}, 8.55] MNm. Details of the input boundaries for *ANN1*, *ANN2* and overall problem are given in Tables 2, 3 and 4, respectively.

Once generated, *Databases 1 and 2* are divided into the train and test sets with the ratio of 0.8/0.2. Consequently, *Databases 1 and 2* have 622/156 and 286/72 samples for train/test sets, respectively. Because there is no strict rule for finding a proper ANN configurations, various ANN architectures have been tried with the aim to minimize the loss function (*MSE* in this study). The process of selecting the best configurations for a machine learning models can be found in many other studies such as [23] or [24] and not provided in this study for the sake of simplicity. The final *ANN1* and *ANN2* models both have five hidden layers; each layer contains 32 nodes and a bias node (as other conventional ANN [49]). With different numbers of output(s), *ANN1* has slightly less weights than that of *ANN2* with 4673 versus 4706 trainable parameters, respectively. The batch size and total epochs for these ANNs are equal to 10 samples and 10^4 epochs. The required training times to develop these models are 380 s for *ANN1* and 261 s for *ANN2*.

Table 2 Descriptive statistics of the generated Database 1 (778 samples)

Variable	Mean	Standard deviation	Min	Max
D	541.7509	425.0669	**100.0000**	**1219.0000**
t/D	0.0419	0.0266	**0.0113**	**0.1000**
d/t	0.5049	0.2406	**0.0000**	**0.8000**
l/D	0.1585	0.0998	**0.0000**	**0.3937**
w_{arc}/D	0.1887	0.0913	**0.0000**	**0.4154**
σ_y	446.8618	80.5888	**290.0000**	**524.0000**
σ_u	582.7224	97.6295	**415.0000**	**701.0000**
ε_y	0.0021	0.0004	**0.0014**	**0.0025**
ε_u	0.0776	0.0218	**0.0430**	**0.1036**
α	2.2656	1.4100	**0.0000**	**π**
N/N_o*	0.0067	0.1722	**− 0.8070**	**0.9120**
M_y/M_x**	0.4195	1.8228	**− 10.0000**	**10.0000**
M_{cap}	2,987,963	3,652,569	0.0000	13,580,000

*N in ANN1 and Database *1* will be equal to N_{cor} in ANN2 and Database *2* which is normalized with N_o where:

$$N_o = \pi\sigma_u\left(\left(\frac{D}{2}\right)^2-\left(\frac{D-2t}{2}\right)^2\right) \quad (4)$$

**The ratio added to observe the cases where defects are out of bending plane

After the training process, observation of *ANN1* and *ANN2* model performance on the train and test sets is shown in Fig. 11 and Table 5. It can be seen from Fig. 11 that both models are appropriate for predicting the interested variables where the data points densely scattered around the 1:1 line. It indicates the minor differences of predicted compared to the simulated values.

The validation metrics in Table 5 reinforce the intuition in Fig. 11 with R^2 in all cases of around 0.99. Compared to the mean values of M_{cap} (1.4025 MNm, Table 2) and M_{peak} (1.305 MNm, Table 3), the errors are consistently less than 0.3 MNm on both train and test sets. The error on N_{cor} is maximum at $RMSE$ = 0.7959MN on the test set (Table 3). The general complexity of the developed models is implicitly measured via the time required to implement a million-sample prediction on Core i5-8250U processor and 16 GB RAM computer. A total of ten case studies are conducted with the mean of time required to predict 10^6 input samples for *ANN1* and *ANN2* which are slightly equal at 10.6375 s and 9.7546 s, respectively. Further observations on computing time for the overall process in Fig. 10 are given in Table 8.

The residuals of interested variables are given in Table 5. It is focused on the test set whose distribution is assumed to be equivalent to the actual distribution of the residuals. The mean values of all residuals (r_{mean}) are close to zero, implying the bias does not occur. It is understandable that the residual standard deviations (r_{std}) are almost equal to the $RMSE$ in all cases. Histograms of residuals are provided in Fig. 12, illustrating the concentration of these values around the zero locations.

The statistical normal tests on the residuals are implemented with conventional methods proposed by D'Agostino [50, 51] and Kolmogorov–Smirnov [52]. The null hypotheses for all the tests are: "The residual follows the normal distribution." The *p-values* of these tests are

Table 3 Descriptive statistics of the generated Database 2 (358 samples)

Variable	Mean	Standard deviation	Min	Max
D (mm)	666.9218	325.6226	**100.0000**	**1200.0000**
t/D	0.0276	0.0179	**0.0053**	**0.0750**
σ_y	448.5000	83.5036	**290.0000**	**524.0000**
σ_u	555.4676	93.2509	**415.0000**	**685.0000**
ε_y	0.0019	0.0004	**0.0014**	**0.0025**
ε_u	0.0775	0.0433	**0.0394**	**0.2230**
f_y/D	-4.3960	3.9072	**− 24.3840**	**0.000**
f_x/D	-0.3684	3.8848	**− 15.9020**	**10.0000**
P_a (N)	37,736	18,560	**12,260**	**75,000**
y_a (mm)	3.0528	1.3330	**1.5000**	**5.0000**
P_t (N)	567,234	258,669	**200,000**	**1,000,000**
y_t (mm)	38.7701	27.8544	**6.7000**	**100.0000**
N_{cor}/N_o*	0.0383	0.0746	**− 0.1371**	**0.2752**
M_{peak}	1,958,532	2,062,205	364	8,550,000
N_{cor}	5,227,779	8,222,423	− 12,700,000	25,300,000

*N_{cor} in *ANN2* and *Database 2* will be equal to N in *ANN1* and *Database 1* which is normalized with N_o in Eq. 4

Table 4 Summarized boundaries of the stress–strength analysis with ANNs

Variable	Min	Max	Variable	Min	Max
D (mm)	100	1200	y_a *(mm)*	1.5	5
t/D	0.0053	0.075	P_t *(N)*	200,000	1,000,000
σ_y *(MPa)*	290	524	y_t *(mm)*	6.7	100
σ_u *(MPa)*	415	685	t/D	0.0113	0.1
ε_y	0.0014	0.0025	d/t	0	0.8
ε_u	0.0394	0.223	l/D	0	0.3937
f_y/D	− 24.384	0.0278	α	0	π
f_x/D	− 15.902	10	N/N_o (or N_{cor}/N_o)	− 0.1371	0.2752
P_a *(N)*	12,260	75,000	M_y/M_x	− 10	10

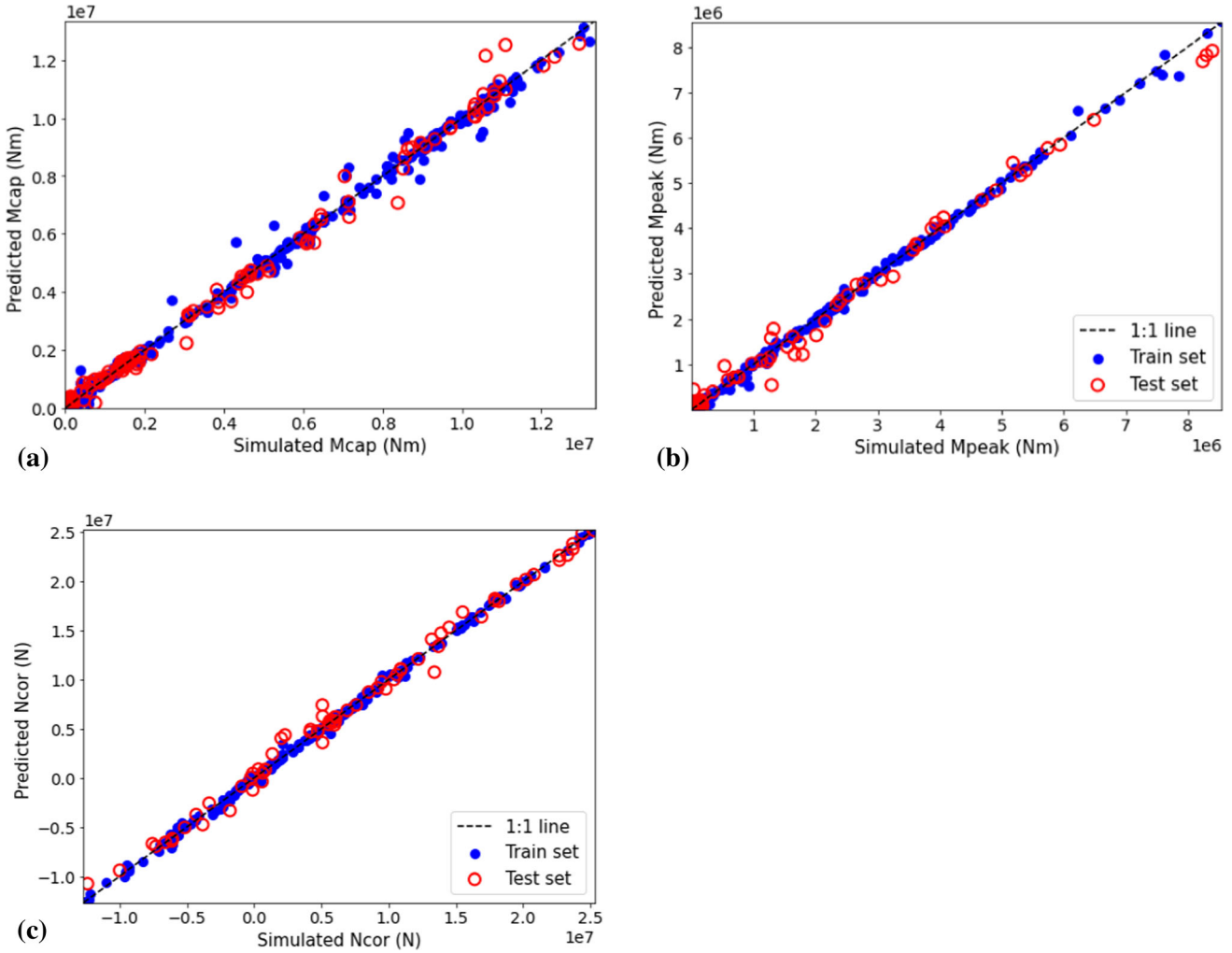

Fig. 11 Comparison of results from the ANN1 (**a**: Mcap) and ANN2 (**b**: Mmax; **c**: Ncor) versus FE simulation

consistently close to zero with the maximum value of 3.1171×10^{-4} (Table 6) larger than 0.01. Consequently, the conclusion can be claimed that: "The null hypotheses cannot be rejected with the confidence level of 0.99." These tests are the fundamentals for obtaining $\widetilde{M}_{\text{cap}}$, $\widetilde{M}_{\text{peak}}$ and $\widetilde{N}_{\text{cor}}$ as in Eqs. 1, 2 and 3 by randomly generated these variables by MCSs (i.e., *MCS1* and *MCS2* in Fig. 10). The comparison of the structure capacity and external force then can be made for each trial to record the number of failure.

Table 5 Validating metrics of proposed ANN model versus other models

Model	Prediction time[a] (second)	Output	Unit	Metric on	R^2	MAE	RMSE	r_{mean}	r_{Std}
ANN1	10.6375	M_{cap}	(MNm)	Train set	0.9973	0.098221	0.187824	0.005769	0.187736
			(MNm)	Test set	0.9943	0.166144	0.289127	**0.008182**[b]	**0.289011**[b]
ANN2	9.7546	M_{peak}	(MNm)	Train set	0.9986	0.046472	0.074232	0.005134	0.074054
			(MNm)	Test set	0.9883	0.159260	0.254812	**0.037552**[c]	**0.252029**[c]
		N_{cor}	(MN)	Train set	0.9989	0.173498	0.264635	− 0.016733	0.264105
			(MN)	Test set	0.9929	0.541692	0.795936	− **0.097199**[d]	**0.789978**[d]

[a]Mean predicting time from 10 cases × 10^6 samples in each case (Table 5; [b]$r_{cap,mean}$ and $r_{cap,std}$; [c]$r_{peak,mean}$ and $r_{peak,std}$; [d]$r_{cor,mean}$ and $r_{cor,std}$

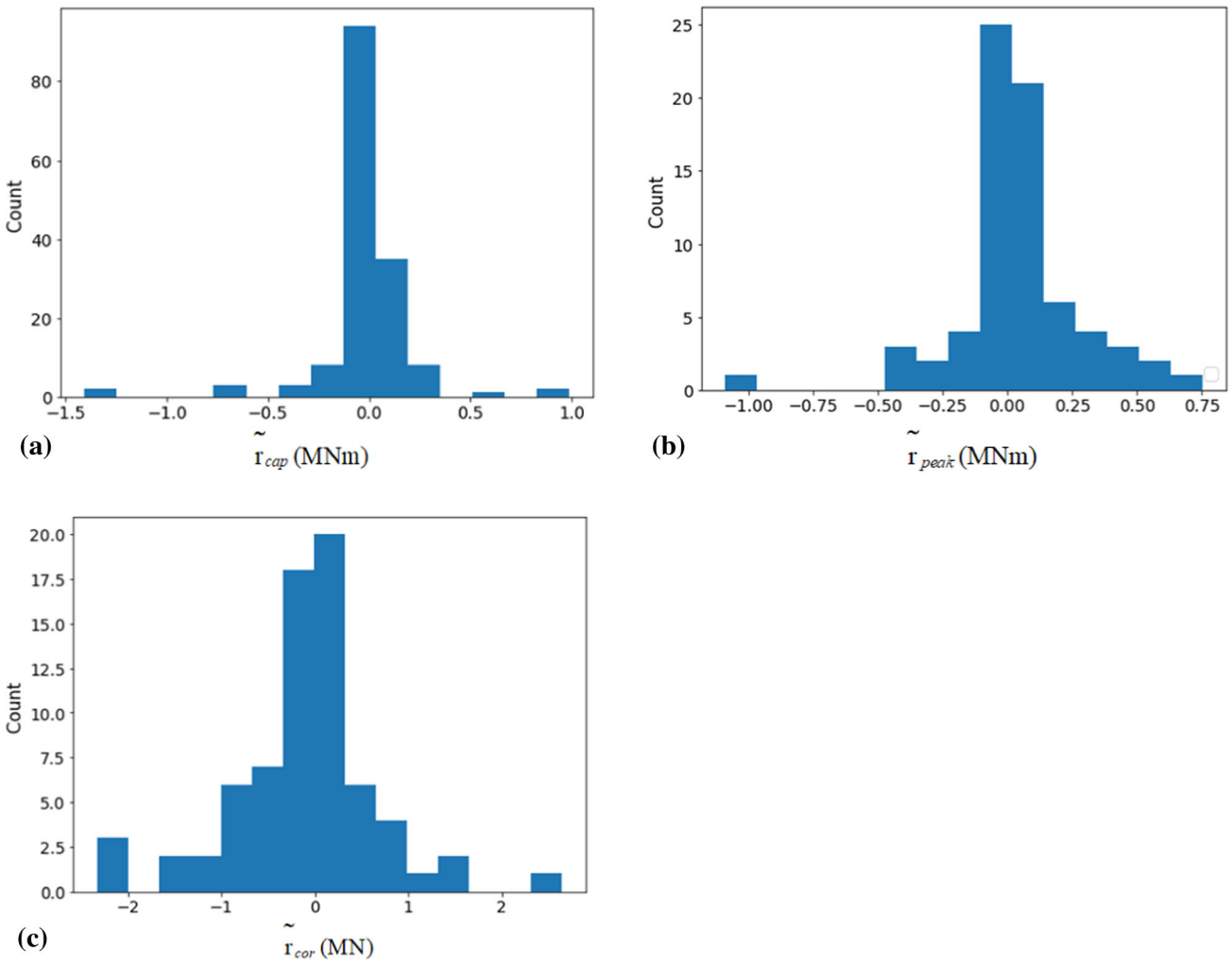

Fig. 12 Histograms of residual of outputs: **a**–**c**

3.2 Failure assessment accounting for model uncertainties

In this section, the framework in Fig. 10 is conducted with a control case given as Case 0 of Table 7. The control case is a pipe made of X42 steel with $D = 762$ mm and $t = 10$ mm. The defect is located in the bending plane ($M_y = 0$), and this flaw is up to 20% of the wall thickness with ratios of length and width of defect to pipe diameter of 0.2 and 0.4, respectively. The fault angle β is $\pi/4$ or f_x/D

Table 6 Test for goodness of fit of output residuals to follow normal distributions

Residual	Test method	*p*-value
$\tilde{r}_{cap}$	D'Agostino [50, 51]	2.0524×10^{-14}
	Kolmogorov–Smirnov [52]	0.0000×10^{-1}
$\tilde{r}_{peak}$	D'Agostino [50, 51]	1.6854×10^{-5}
	Kolmogorov–Smirnov [52]	8.2681×10^{-24}
$\tilde{r}_{cor}$	D'Agostino [50, 51]	3.1171×10^{-4}
	Kolmogorov–Smirnov [52]	3.5229×10^{-18}

and f_y/D are equal at 1. The negative signal in f_y/D indicates the reversed displacement direction described in Fig. 6. The transverse soil springs have yield force at $P_T = 0.537$ MN, and this value of axial direction P_a is 0.01226 MN. The $M_{\text{peak,pred}}$ and $N_{\text{cor,pred}}/N_o$ are obtained from *ANN2* for this case of 0.71440 and 0.0313, respectively. The value of $N_{\text{cor,pred}}/N_o$ is then used along with other required inputs for *ANN1*. It is calculated that the moment capacity of the defected pipe, $M_{\text{cap,pred}}$, is 1.84725 MNm. With pipe capacity which is almost triple the external force, the deterministic approach claims a safe status. However, with the appearance of model uncertainties, the failure probability of the structure, P_f, is 0.00253. To obtain this probability, each MCS in Fig. 10 is implemented with 10^6 trials.

Comparing the control Case 0 to Cases 1–9, a selective parametric study of the problem is conducted. In Case 1, pipe diameter D decreases to 500 mm, while other absolute inputs are the same. (The relative inputs changed due the change of normalized value D.) This change leads to reduction of $M_{\text{cap,pred}}$ from 1.8475 MNm to 1.02611 MNm and $M_{\text{peak,pred}}$ from 0.71440 MNm to 0.56304 MNm. Meanwhile, relative external force, $N_{\text{cor,pred}}$, increased from 0.03130 to 0.04117. Consequently, the failure probability of the pipe jumped up to 0.12724.

In the cases where both $M_{\text{cap,pred}}$ and $M_{\text{peak,pred}}$ are increased, failure probability, P_f, may increase or decrease depending on the changing quantities of these moments. For instance, if the wall thickness is double from 10 to 20 mm (Case 2), $M_{\text{cap,pred}}$ raises to 2.18546 MNm. However, the increase in pipe stiffness with thicker wall leads to the triple of $M_{\text{peak,pred}}$ to 2.4954 MNm. To the end, the pipe is predicted to have 80.758 percent of failure.

Analogously, if the defect is propagated deeper from 0.2 to 0.5 to wall thickness, the failure probability is 0.01428 (Case 3). In Case 4, if the defect is out of the bending plane with an angle of $\beta = \pi/4$, $M_{\text{cap,pred}}$ is slightly increased to 1.89197 MNm and thus P_f is reduced to 0.00159.

The improvement in pipe material from X42 steel to X80 steel in Case 5 is an interesting case. The use of higher grade leads to the lower reliability of the pipe. In this case, $M_{\text{cap,pred}}$ is significantly increased to 2.18095 MNm. However, the dramatic increase of $M_{\text{peak,pred}}$ from 0.71440 MNm to 3.78329 MNm causes exploding of P_f to 99.999%. This phenomenon is likely due to the higher stiffness of X80 at the hardening state $E_2 = 2132$ MPa compared to this of X42 ($E_2 = 1223$ MPa) as in Table 1.

In Case 6, the absence of soil axial displacement, f_x/D, leads to the significant increase of P_f to 0.01504. Meanwhile, if β is constant and the quantity of the fault displacement is triple, the failure probability slightly increases to 0.00717 (Case 7). This illustrates the positive effect of f_x/D to the safety of the pipe.

Besides, the increase of P_a from 0.012260 MN to 0.02 MN is positively correlated with the improvement of $M_{\text{cap,pred}}$ to 1.85088 MNm (Case 8). Along with the dramatic reduction of $M_{\text{peak,pred}}$ to 0.03547 MNm and the axial force increase to 0.04095 MN, the failure probability in this case is zero. In Case 9, if the stiffness of the soil is improved in the transverse direction from 0.53700 MN to 0.80000 MN, the structure is likely to be broken with P_f of up to 0.93655. This is because the hard soil will reduce the anchor length of pipe. Consequently, the external moment is concentrated within a shorter length with the same displacement.

Additional information on the time required for implementing Cases ID 0–9 is given in Table 8. Along with the overall time to conduct the process in Fig. 10, the decompositions are also provided. The components are: predicting times of *ANN1*, *ANN2* (not included in the overall estimation) and other necessary steps such as generating random data for MCSs, assessing the failure probability, etc. It generally takes 14.6544 s for conducting the overall problem which assesses the failure probability of defected pipe under strike-slip fault. Because only one prediction on *ANN2* is required to obtain $M_{\text{peak,pred}}$ and $N_{\text{cor,pred}}$, running time for *ANN2* is not included in the overall assessment. On average, predicting with 10^6 *ANN1* predictions accounts for 72.59% to the total computing time (step 7 in the pseudo-code). The remaining steps 1–6 and 8–11 in the pseudo-code take 27.41% the total time (i.e., 4.0169 s on average).

4 Conclusion and discussion

The paper proposed an approach for the stress–strength problem of the defected pipe under the strike-slip fault. *ANN1* and *ANN2* models have been developed based on *Database 1* (778 samples) and *Database 2* (358 samples) from FEAs, respectively. The validating metrics on train and test set are investigated with the R^2*s* of around 0.99, and errors (i.e., *MEA* and *RMSE*) are substantially low.

Table 7 Prediction with ANN models accounting for the uncertainties

Variable		Case id									
		0*	1	2	3	4	5	6	7	8	9
Inputs	*D* (mm)	762	**500↓**	762	762	762	762	762	762	762	762
	t/D	0.01312	0.02000	**0.02625↑**	0.01312	0.01312	0.01312	0.01312	0.01312	0.01312	0.01312
	d/t	0.20000	0.13123	0.10000	**0.50000↑**	0.20000	0.20000	0.20000	0.20000	0.20000	0.20000
	l/D	0.20000	0.13123	0.20000	0.20000	0.20000	0.20000	0.20000	0.20000	0.20000	0.20000
	w_{arc}/D	0.40000	0.26247	0.40000	0.40000	0.40000	0.40000	0.40000	0.40000	0.40000	0.40000
	Grade	X42	X42	X42	X42	X42	**X80↑**	X42	X42	X42	X42
	α	π	π	π	π	π	π	π	π	π	π
	M_y/M_x	0.00000	0.00000	0.00000	0.00000	**1.00000↑**	0.00000	0.00000	0.00000	0.00000	0.00000
	f_y/D	− 1.00000	− 0.65617	− 1.00000	− 1.00000	− 1.00000	− 1.00000	− 1.00000	**− 3.0000↑**	− 1.00000	− 1.00000
	f_x/D	1.00000	0.65617	1.00000	1.00000	1.00000	1.00000	**0.00000↓**	**3.0000↑**	1.00000	1.00000
	P_a (MN)	0.01226	0.01226	0.01226	0.01226	0.01226	0.01226	0.01226	0.01226	**0.02000↑**	0.01226
	y_a (mm)	3.8	3.8	3.8	3.8	3.8	3.8	3.8	3.8	3.8	3.8
	P_t (MN)	0.53700	0.53700	537,000	0.53700	0.53700	0.53700	0.53700	0.53700	0.53700	**0.80000↑**
	y_t (mm)	33.0	33.0	33.0	33.0	33.0	33.0	33.0	33.0	33.0	33.0
	$N_{cor,mean}/N_o$	0.03130	0.04117↑	0.03149↑	0.03130-	0.03130-	− 0.00734↓	0.02467↓	0.03278↑	0.04095↑	− 0.00212↓
Outputs	$M_{peak,mean}$ (MNm)	0.71440	0.56304↓	2.49544↑	0.71440-	0.71440-	3.78329↑	0.95752↑	0.85184↑	0.03547↓	2.37777↑
	$M_{cap,mean}$ (MNm)	1.84725	1.02611↓	2.18546↑	1.62462↓	1.89197↑	2.18095↑	1.84475-	1.84781↑	1.85088↑	1.83729↑
	P_f	**0.00253**	**0.12724↑**	**0.80758↑**	**0.01428↑**	**0.00159↓**	**0.99999↑**	**0.01504↑**	**0.00717↑**	**0.00000↓**	**0.93655↑**

*Control case

Table 8 Required time for conducting overall model on 10^6 samples MCSs

Case ID	Predicting time (s) requirement for:			
	ANN1	*ANN2*[a]	Other[b]	Overall (*ANN1* + Other)
0	10.7554	10.2825	4.0593	14.8147
1	11.3195	9.8307	4.0907	15.4102
2	11.1063	10.2857	4.1569	15.2632
3	10.9609	9.5365	3.9343	14.8952
4	10.918	9.3547	4.0502	14.9682
5	11.1105	9.5665	3.9879	15.0984
6	10.0393	9.0398	3.988	14.0273
7	10.0675	10.2103	3.9515	14.019
8	10.2202	9.1989	3.9206	14.1408
9	9.8773	10.2406	4.0295	13.9068
Mean:	10.6375	9.7546	4.0169	14.6544

[a]Not included in the overall prediction

[b]Other steps of the overall model in Fig. 10 and pseudo-code, such as generating random input data for *MSC1* and *2*, calculating P_f, etc.

Additionally, the model uncertainties of the overall prediction are accounted for with the assumption that the actual distribution of models residuals and this on test set are equivalent. Consequently, MCS can be conducted with the randomness of outputs extracted from residuals on the test set. The uncertainty of *ANN1* is presented via residual mean, $r_{\text{cap,mean}} = 0.0082$ MNm, and standard deviation, $r_{\text{cap,std}} = 0.2890$ MNm. Meanwhile, means and standard deviations of *ANN2* are $r_{\text{peak,mean}} = 0.0376$ MNm, $r_{\text{peak,std}} = 0.2520$ MNm for predicting the peak moment and $r_{\text{cor,mean}} = -0.0972$ MN, $r_{\text{cor,std}} = 0.7898$ MN for the corresponding axial force. The transformation of deterministic input to the probability of failure at the end of the overall model reflexes the uncertainty of models in terms of probability.

Simultaneously, time complexity of constituent models and the overall model is observed based on the running time of the overall model and constituent models. The acceptable overall running time (around 14.64 s, including the *MCS1* and *MCS2*) on a computer with low-medium power indicates the practical application of the proposed framework.

Based on the quantification of model uncertainty, the selective parametric study is also provided revealing the hidden relationship between inputs and output. For instance, the stiffness of pipe is important to the formation of the external forces, and the increase in the transverse yield force leads to more severe scenario.

The paper can be extended with the expansion of number of the samples for each database. The main purpose of this improvement is to widen the boundaries naturally set by the minimum and maximum of each input. For example, other materials can be included, or the normal fault crossing problem can be additionally considered. The proposed method and the parametric study also suggest some further works on an optimization. But the increase in pipe dimensions not only improves moment capacity but also causes a larger external forces due to the increase in pipe stiffness.

Acknowledgements This research was funded by Vietnam National Foundation for Science and Technology Development (NAFOSTED) under Grant number: 107.02-2020.04.

Data availability The raw/processed data required to reproduce these findings will be made available on request.

Declarations

Conflicts of interest The authors declare that they have no conflict of interest.

References

1. Karamitros DK, Bouckovalas GD, Kouretzis GP (2007) Stress analysis of buried steel pipelines at strike-slip fault crossings. Soil Dyn Earthq Eng 27(3):200–211
2. Karamitros DK et al (2011) An analytical method for strength verification of buried steel pipelines at normal fault crossings. Soil Dyn Earthq Eng 31(11):1452–1464
3. Talebi F, Kiyono J (2020) Introduction of the axial force terms to governing equation for buried pipeline subjected to strike-slip fault movements. Soil Dyn Earthq Eng 133:106125
4. Liu X et al (2020) A refined analytical strain analysis method for offshore pipeline under strike-slip fault movement considering strain hardening effect of steel. Ships Offshore Struct 15(2):215–226
5. Huan DT, Tu TM, Quoc TH (2017) Analytical solutions for bending, buckling and vibration analysis of functionally graded cylindrical panel. Vietnam J Sci Technol 55(5):587
6. Trifonov OV (2018) The effect of variation of soil conditions along the pipeline in the fault-crossing zone. Soil Dyn Earthq Eng 104:437–448
7. Melissianos VE et al (2016) Numerical evaluation of the effectiveness of flexible joints in buried pipelines subjected to strike-slip fault rupture. Soil Dyn Earthq Eng 90:395–410
8. Melissianos VE, Gantes CJ (2017) Numerical modeling aspects of buried pipeline—fault crossing. In: Lagaros ND, Papadrakakis M, Plevris V (eds) Computational methods in earthquake engineering. Springer, Cham, pp 1–26
9. Vazouras P, Karamanos SA, Dakoulas P (2010) Finite element analysis of buried steel pipelines under strike-slip fault displacements. Soil Dyn Earthq Eng 30(11):1361–1376
10. Zhang J, Xiao Y, Liang Z (2018) Mechanical behaviors and failure mechanisms of buried polyethylene pipes crossing active strike-slip faults. Compos B Eng 154:449–466
11. Vazouras P, Dakoulas P, Karamanos SA (2015) Pipe–soil interaction and pipeline performance under strike—slip fault movements. Soil Dyn Earthq Eng 72:48–65

12. Trifonov OV, Cherniy VP (2010) A semi-analytical approach to a nonlinear stress–strain analysis of buried steel pipelines crossing active faults. Soil Dyn Earthq Eng 30(11):1298–1308
13. Uckan E et al (2015) A simplified analysis model for determining the seismic response of buried steel pipes at strike-slip fault crossings. Soil Dyn Earthq Eng 75:55–65
14. Folkman S (2018) Water main break rates in the USA and Canada: a comprehensive study. Mechanical and Aerospace Engineering Faculty Publications, Paper 174
15. Phan HC, Dhar AS, Mondal BC (2017) Revisiting burst pressure models for corroded pipelines. Can J Civ Eng 44(7):485–494
16. Nunes L, Nascimento V (2011) Estimation of internal defect size by means of radial deformations in pipes subjected to internal pressure. Thin-Walled Struct 49(2):298–303
17. Keshtegar B, Seghier MAB (2018) Modified response surface method basis harmony search to predict the burst pressure of corroded pipelines. Eng Fail Anal 89:177–199
18. Amaya-Gómez R et al (2019) Reliability assessments of corroded pipelines based on internal pressure—a review. Eng Fail Anal 98:190–214
19. Mondal BC, Dhar AS (2019) Burst pressure of corroded pipelines considering combined axial forces and bending moments. Eng Struct 186:43–51
20. Liu J et al (2009) Remaining strength of corroded pipe under secondary (biaxial) loading. GL Industrial Services UK Ltd., Loughborough, UK
21. Peng J et al (2011) Safety assessment of pipes with multiple local wall thinning defects under pressure and bending moment. Nucl Eng Des 241(8):2758–2765
22. Zhao Z et al (2018) Influence of pitting corrosion on the bending capacity of thin-walled circular tubes. J Braz Soc Mech Sci Eng 40(11):548
23. Phan HC et al. (2020) Predicting capacity of defected pipe under bending moment with data-driven model. In: International conference on modern mechanics and applications. Lecture notes in mechanical engineering, Springer: Ho Chi Minh city, Vietnam.
24. Phan HC, Duong HT (2021) Predicting burst pressure of defected pipeline with principal component analysis and adaptive neuro fuzzy inference system. Int J Press Vessels Pip 189:104274
25. Duong HT et al (2020) Optimization design of rectangular concrete-filled steel tube short columns with balancing composite motion optimization and data-driven model. in structures. Elsevier
26. Le TT (2020) Practical machine learning-based prediction model for axial capacity of square CFST columns. Mech Adv Mat Struct 2020:1–16
27. Le TT, Phan HC (2020) Prediction of ultimate load of rectangular CFST columns using interpretable machine learning method. Adv Civil Eng 2020:8855069
28. Le T-T, Le MV (2021) Development of user-friendly kernel-based Gaussian process regression model for prediction of load-bearing capacity of square concrete-filled steel tubular members. Mater Struct 54(2):1–24
29. Soize C et al. (2015) Stochastic representations and statistical inverse identification for uncertainty quantification in computational mechanics. In: (Plenary Lecture) UNCECOMP 2015, 1st ECCOMAS thematic international conference on uncertainty quantification in computational sciences and engineering
30. Phan HC, Dhar AS (2021) Predicting pipeline burst pressures with machine learning models. Int J Press Vessels Piping 191:104384
31. Phan HC et al (2021) An empirical model for bending capacity of defected pipe combined with axial load. Int J Press Vessel Piping 191:104368
32. Mondal BC, Dhar AS (2018) Improved Folias factor and burst pressure models for corroded pipelines. J Press Vessel Technol. https://doi.org/10.1115/1.4038720
33. Shuai Y, Shuai J, Zhang X (2018) Experimental and numerical investigation of the strain response of a dented API 5L X52 pipeline subjected to continuously increasing internal pressure. J Nat Gas Sci Eng 56:81–92
34. Diniz J et al (2006) Stress and strain analysis of pipelines with localized metal loss. Exp Mech 46(6):765–775
35. Oh C-K et al (2007) Ductile failure analysis of API X65 pipes with notch-type defects using a local fracture criterion. Int J Press Vessels Pip 84(8):512–525
36. Ma B et al (2013) Assessment on failure pressure of high strength pipeline with corrosion defects. Eng Fail Anal 32:209–219
37. Zheng M et al (2004) Modified expression for estimating the limit bending moment of local corroded pipeline. Int J Press Vessels Pip 81(9):725–729
38. Chen Y et al (2014) Residual bending capacity for pipelines with corrosion defects. J Loss Prev Process Ind 32:70–77
39. Trifonov OV, Cherniy VP (2012) Elastoplastic stress–strain analysis of buried steel pipelines subjected to fault displacements with account for service loads. Soil Dyn Earthq Eng 33(1):54–62
40. Tahghighi H, Hajnorouzi M (2014) Numerical evaluation of the strike-slip fault effects on the steel buried pipelines. J Seismol Earthq Eng 16(4):219
41. Melissianos VE, Gantes CJ (2015) Failure mitigation of buried steel pipeline under strike-slip fault offset using flexible joints. In: SECED 2015 Conference: Earthquake Risk and Engineering towards a Resilient World
42. Liu X et al (2016) A semi-empirical model for peak strain prediction of buried X80 steel pipelines under compression and bending at strike-slip fault crossings. J Nat Gas Sci Eng 32:465–475
43. Gas ASoCECo, Lifelines LF (1984) Guidelines for the seismic design of oil and gas pipeline systems. Am Soc Civil Eng
44. Zolfaghari A, Izadi M (2020) Burst pressure prediction of cylindrical vessels using artificial neural network. J Press Vessel Technol 142(3):031303
45. Oh D et al (2020) Burst pressure prediction of API 5L X-grade dented pipelines using deep neural network. J Marine Sci Eng 8(10):766
46. Keshtegar B, Miri M (2014) Reliability analysis of corroded pipes using conjugate HL–RF algorithm based on average shear stress yield criterion. Eng Fail Anal 46:104–117
47. Keshtegar B, Meng Z (2017) A hybrid relaxed first-order reliability method for efficient structural reliability analysis. Struct Saf 66:84–93
48. Keshtegar B et al (2019) Reliability analysis of corroded pipelines: novel adaptive conjugate first order reliability method. J Loss Prev Process Ind 62:103986
49. Géron A (2019) Hands-on machine learning with Scikit-Learn, Keras, and TensorFlow: concepts, tools, and techniques to build intelligent systems. O'Reilly Media
50. d'Agostino RB (1971) An omnibus test of normality for moderate and large size samples. Biometrika 58(2):341–348
51. D'agostino R, Pearson ES (1973) Tests for departure from normality. empirical results for the distributions of b 2 and$\sqrt{}$ b. Biometrika 60(3):613–622
52. Massey FJ Jr (1951) The Kolmogorov-Smirnov test for goodness of fit. J Am Stat Assoc 46(253):68–78